Eur. Phys. J. B (2013) 86: 25
DOI: 10.1140/epjb/e2012-30521-4

THE EUROPEAN PHYSICAL JOURNAL B

Regular Article

From the inverted pendulum to the periodic interface modes

Nicolas Combe[1,2,a]

[1] Centre d'Elaboration de Matériaux et d'Etudes Structurales, CNRS UPR 8011, 29 rue J. Marvig, BP 94347, 31055 Toulouse cedex 4, France
[2] Université de Toulouse, UPS, 31055 Toulouse, France

Received 27 June 2012 / Received in final form 24 October 2012
Published online 28 January 2013 –

Abstract. The physics of the spatial propagation of monochromatic waves in periodic media is related to the temporal evolution of the parametric oscillators. We transpose the possibility that a parametric pendulum oscillates in the vicinity of its unstable equilibrium position to the case of monochromatic waves in a lossless unidimensional periodic medium. We develop this concept, that can formally applies to any kind of waves, to the case of longitudinal elastic wave. Our analysis yields us to study the propagation of monochromatic waves in a periodic structure involving two main periods. We evidence a class of phonons we refer to as periodic interface modes that propagate in these structures. These modes are similar to the optical Tamm states exhibited in photonic crystals. Our analysis is based on both a formal and an analytical approach. The application of the concept to the case of phonons in an experimentally realizable structure is given. We finally show how to control the frequencies of these phonons from the engineering of the periodic structure.

Waves in periodic media have focused the interest of many scientists and have found numerous applications (mirrors, filters, etc.) in different branches of physics: phonons (elastic waves) in crystalline solids or in phononic crystals [1], electromagnetic (EM) waves in photonic crystals [2], electron wave functions in crystalline solids [3] or electronic superlattices [4]. An essential property of the waves propagation in these structures is the existence of band gaps (BG) in which the amplitude of a monochromatic wave exponentially varies, hence corresponding to non-physical states in infinite media. Outside of these gaps, monochromatic waves are spatially (pseudo-) periodic.

In phononic crystals, derived from the existence of Rayleigh and Stoneley waves associated to a surface or an interface, an unconventional type of acoustic waves has been exhibited in superlattices (SL) [5–7] or related structures [8]. Provided a component of the wave vector parallel to the SL interfaces (in-plane wave vector) different from zero, the spatial dependence perpendicular to the interfaces of the wave function (displacement) is a pseudo-periodic function displaying a succession of growing and decreasing exponentials in each layer of the SL, the amplitude of the wave function being bounded. The wave function of this unconventional type of acoustic waves thus present a high amplitude in the vicinity of some interfaces and are thus periodically localized at these interfaces.

Concerning optical phonons, an analogous unconventional wave has been evidenced, namely interface optical phonons. Interface optical phonons with a wave vector perpendicular to the SL interfaces (zero in-plane wave vector) have been experimentally evidenced in a GaAs-AlAs SL by Raman scattering [9]. Their frequencies fall in the BG of the SL, and their wave functions display a succession of growing and decreasing exponentials in each subset of the SL [10].

Some different though related unconventional waves have been exhibited in photonic crystals: their wave functions are composed of an oscillating function whose amplitude displays a succession of growing and decreasing exponentials in a photonic crystal. Contrary to the unconventional phonons derived from the Rayleigh and Stoneley waves, these modes can propagate in a periodic unidimensional structure with a zero in-plane wave vector. A coupled resonator optical wave guide (CROW) [11,12], a photonic crystal presenting some periodic impurities (the resonator or cavities) can support the propagation of such modes. If the size of the cavities is judiciously chosen, some waves falling in the BG of the photonic crystal can propagate through the CROW with a zero in-plane wave vector: the cavities are thus coupled through oscillating waves with evanescent amplitudes. Structures made of two conjugated SLs [13] and of two different semi-infinite photonic crystals with a common interface and with overlapping BG [14] have also been shown to support the propagation of these unconventional modes. In this latter case, these unconventional modes are called optical Tamm states. The amplitudes of these modes are evanescent in each photonic crystal. Optical Tamm states have been experimentally evidenced [15,16] in finite structures.

In this manuscript, a general physical interpretation of these latter unconventional modes is given. The equivalence [17] between the physics of the spatial

[a] e-mail: combe@cemes.fr

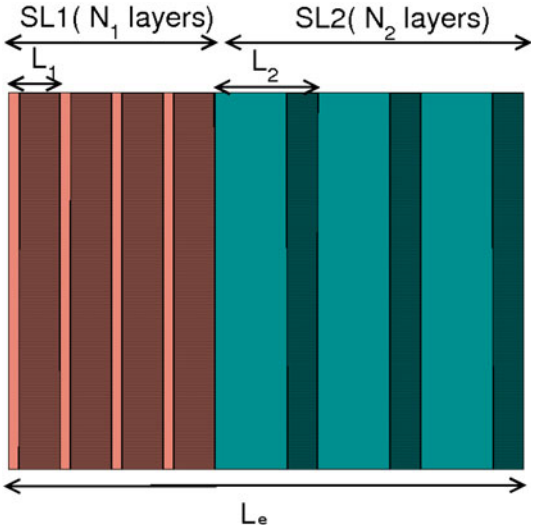

Fig. 1. (Color online) Sketch of the elementary cell of a SSL (unit cell "ABABABABCDCDCD"). The dark green and red background colors correspond to the SL1 (unit cell of the type "AB") and SL2 (unit cell of the type "CD") regions: dark green, dashed dark green, red and dashed red regions, respectively represent A,B,C,D materials.

propagation of monochromatic waves in a lossless unidimensional infinite periodic (LUIP) medium and the one of the temporal evolution of the parametric oscillator in classical mechanics is exploited to evidence the unconventional waves analogous to optical Tamm states: these waves can be considered as the transposition of the striking possibility for an oscillator to oscillate in the vicinity of an unstable equilibrium position using a parametric excitation (for instance in the inverted pendulum experiment). Since, to our knowledge, such modes analogous to optical Tamm states, have never been reported in the case of elastic waves propagating in an unidimensional structure, the propagation of elastic waves (with a zero in-plane wave vector) in SL will be considered here.

The transposition of the inverted pendulum experiment to the case of phonons in an unidimensional structure, yields us to consider the propagation of a monochromatic wave in a periodic structure involving two main (judiciously chosen) periods: a SL whose unit cell (e.g. a unit cell of the type "ABABABABCDCDCD") contains two finite periodic subsets (e.g. "ABABABAB" and "CDCDCD") having some overlapping regions of their BG is an example of such medium (see also [18]). In the following, such SL will be referred as a supersuperlattice (SSL). The sketch of the elementary unit cell of a SSL is depicted in Figure 1. The unconventional type of monochromatic waves, referred as periodic interface modes (PIM) in this work will be studied and described: they propagate in a SSL while their frequencies belong to an overlapping region of the BG of each subset (e.g. "ABABABAB" and "CDCDCD"). The amplitude of such waves exponentially varies in each subset in an opposite way, but exhibits a sinusoidal envelope in the whole structure.

In Section 1, the equivalence between the spatial propagation of phonons in a LUIP medium and the temporal evolution of a parametric oscillator is detailed. Transposing the possibility for a parametric oscillator to oscillate in the vicinity of an unstable equilibrium position, some heuristic arguments why to consider the propagation of waves in a periodic structure involving two main periods are provided. In Section 2, using a formal expression of the wave equation, an analytic framework that yields an approximated analytical expression of the wave function for the PIM is given. In Section 3, the preceding analysis is applied to the case of the propagation of phonons in achievable structures. Finally, Section 4 is devoted to the discussion.

1 Heuristic arguments

1.1 The wave propagation in a LUIP medium and the parametric oscillator

As exploited recently [17], the physics of the propagation of a monochromatic wave in a LUIP medium is equivalent to that of the temporal evolution of a parametric oscillator. In the following, all considered waves are monochromatic.

Let us consider the propagation of an elastic wave in a LUIP medium (direction z, period λ_s). In addition, the case of a longitudinal elastic wave with normal incidence (zero in-plane wave vector) is considered. Using the linear elasticity theory [19], the displacement field associated to an elastic wave of angular frequency ω writes $\boldsymbol{U}(z,t) = \mathfrak{U}(z,\omega)e^{i\omega t}\boldsymbol{z}$ and is solution of the Navier equation:

$$C(z)\frac{d^2\mathfrak{U}}{dz^2}(z,\omega)+\frac{dC}{dz}(z)\frac{d\mathfrak{U}}{dz}(z,\omega)+\rho(z)\omega^2\mathfrak{U}(z,\omega)=0, \quad (1)$$

where $C(z)$ and $\rho(z)$ are the elastic coefficient c^{zzzz} (or C_{33} using the Voigt notation) and the mass density, respectively. Setting $\mathfrak{U}(z,\omega) = Q(z,\omega)u(z,\omega)$ with $Q(z,\omega)$ satisfying $2C\frac{dQ}{dz} + \frac{dC}{dz}Q = 0$, $u(z,\omega)$ is solution of:

$$\frac{d^2u}{dz^2}(z,\omega) + p(z,\omega)u(z,\omega) = 0, \quad (2)$$

where $p(z,\omega) = \frac{\rho\omega^2}{C} - \frac{1}{2C}\frac{d^2C}{dz^2} + \frac{1}{4C^2}[\frac{dC}{dz}]^2$.

In a LUIP medium, the function $p(z,\omega)$ in equation (2) is real and periodic (period λ_s and wave number $k_s = \frac{2\pi}{\lambda_s}$). Equation (2) is a Hill equation. The qualitative behaviour of the solutions of equation (2) can be deduced from a peculiar case of the Hill equation, the Mathieu equation: equation (2) reduces to a Mathieu equation by considering a sinusoidal variation of $p(z,\omega)$ or limiting the Fourier series of $p(z,\omega)$:

$$p(z,\omega) \approx p_0(\omega) + p_1(\omega)\cos(k_s z) \quad (3)$$

$$\Longrightarrow \frac{d^2u}{d\tilde{z}^2}(\tilde{z}) + [\tilde{\eta}_0(\omega) + 2\tilde{\alpha}(\omega)\cos(2\tilde{z})]u(\tilde{z}) = 0, \quad (4)$$

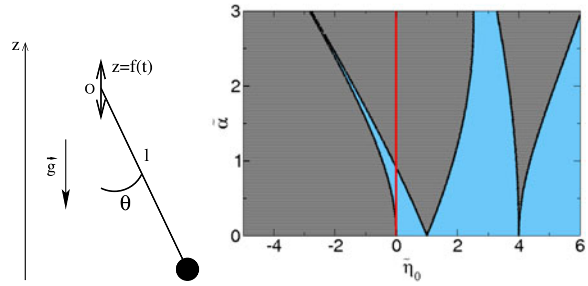

Fig. 2. (Color online) (a) Sketch of a parametric pendulum, (b) phase diagram of equation (6). (Pseudo-) periodic and exponential solutions are in blue and dashed regions. A vertical red line points up $\tilde{\eta}_0 = 0$.

where $\tilde{\eta}_0(\omega) = \frac{4p_0(\omega)}{k_s^2}$ is a positive quantity, $\tilde{\alpha}(\omega) = \frac{2p_1(\omega)}{k_s^2}$, $\tilde{z} = \frac{k_s z}{2}$ and where the dependence of u on ω has been dropped for clarity reasons. Equation (4) is a Mathieu equation. In the following, all dimensionless quantities (or in reduced unit) will have an over-tilde.

Provided that one interprets the space variable $\tilde{z}$ in equation (4) as a time variable, equation (4) for the spatial propagation of waves is similar to the temporal evolution equation of a parametric oscillator. A common example of a parametric oscillator is a simple pendulum whose suspension point has a vertical motion $z = f(t)$, with f a periodic function (angular frequency ω_s): see Figure 2a. The study of the stability of its fixed points θ_0 yields the following Hill equation for the deviation $u = \theta - \theta_0$ with θ the angle of the pendulum:

$$l\frac{d^2u}{dt^2} + \epsilon\left[g + \frac{d^2 f(t)}{dt^2}\right] u = 0, \tag{5}$$

where l and g are, respectively, the length of the pendulum and the standard gravity. The state of the pendulum is characterized by $\boldsymbol{u} = (u, \frac{du}{dt})$. In equation (5), $\epsilon = 1$ for the study of the stable fixed point $\theta_0 = 0$ and $\epsilon = -1$ for the unstable one $\theta_0 = \pi$. Equation (5) reduces to the Mathieu equation when the parametric excitation is sinusoidal $z = -z_0 \cos(\omega_s t)$:

$$\frac{d^2u}{d\tilde{t}^2} + \left[\tilde{\eta}_0 + 2\tilde{\alpha}\cos(2\tilde{t})\right] u = 0, \tag{6}$$

with $\tilde{t} = \frac{\omega_s t}{2}$, $\tilde{\eta}_0 = \epsilon\frac{4\omega_0^2}{\omega_s^2}$ and $\tilde{\alpha} = \epsilon 2z_0/l$ and where $\omega_0^2 = g/l$, ω_s and z_0 are, respectively, the pendulum eigen angular frequency, the excitation angular frequency and amplitude. $\tilde{\eta}_0$ is positive around the fixed point $\theta_0 = 0$ and negative around $\theta_0 = \pi$.

Provided the change $\tilde{z} \leftrightarrow \tilde{t}$ ($k_s \leftrightarrow \omega_s$), equations (4) and (6) are equivalent: their solutions are thus also equivalent.

Using a time translation $\tilde{t} \to \tilde{t} + \frac{\pi}{2}$, the study of the solutions of equation (6) can be reduced to the case $\tilde{\alpha} > 0$. Depending on $\tilde{\eta}_0$ and $\tilde{\alpha}$, the solutions of equation (6) are either (pseudo-) periodic or exponential. The (pseudo-) periodic solutions correspond to a (pseudo-) periodic variation of the angle of the pendulum (solutions of Eq. (6)) and to propagative modes in the case of waves (solutions of Eq. (4)). The exponential solutions are oscillating functions with an exponentially varying amplitude: they correspond to the parametric resonances for the parametric pendulum and to modes in the BG for the waves.

Mathematically, using the Floquet theory, the (pseudo-) periodic and exponential solutions are associated to eigenvalues of $\mathbf{R}_0^{\pi}$ of module respectively equal to and different from 1 [20], with $\mathbf{R}_{\tilde{t}_0}^{\tilde{t}}$ the propagator of equation (6): $\boldsymbol{u}(\tilde{t}) = \mathbf{R}_{\tilde{t}_0}^{\tilde{t}}\,\boldsymbol{u}(\tilde{t}_0)$. The phase diagram of equation (6), obtained by numerically calculating the propagator of equation (6) is reported in Figure 2b.

For the parametric pendulum, both $\tilde{\eta}_0 > 0$ (stability of the fixed point $\theta_0 = 0$) and $\tilde{\eta}_0 < 0$ (stability of the fixed point $\theta_0 = \pi$) regions are relevant. Remarkably, in Figure 2b, the parametric pendulum evidences some (pseudo-) periodic solutions in the $\tilde{\eta}_0 < 0$ region i.e. in the vicinity of $\theta_0 = \pi$, corresponding to the inverted pendulum experiment [21]. Since $\tilde{\eta}_0 > 0$ in equation (4), such mathematical (pseudo-) periodic solutions in the $\tilde{\eta}_0 < 0$ region are not physically relevant in the case of wave.

Note that allowing a non zero in-plane wave vector, surface (Rayleigh) or interface (Stoneley) elastic waves can display a negative value $\tilde{\eta}_0$ in the direction perpendicular to the SL interfaces: the study of such a case has been already reported in the literature [5,8]. Besides, the same derivation can be performed in the case of electromagnetic waves: $\tilde{\eta}_0$ is then proportional to the relative dielectric permittivity. For a metal below the plasma frequency, the (real part of the) relative dielectric permittivity is negative resulting in a negative value of $\tilde{\eta}_0$ in equation (6). However, the dielectric permittivity of a metal is a complex quantity whose imaginary part is related to the absorption and cannot be neglected. The case of complex values of $\tilde{\eta}_0$ is out of the scope of this study.

In the following, the study is limited to the case of elastic waves with normal incidence for which $\tilde{\eta}_0 > 0$. As a consequence, the following study will be easily transposable to any kind of waves.

1.2 Transposing the inverted pendulum case to the wave propagation in LUIP media

Despite the previous analysis, it is possible to design a LUIP medium where some waves, analogous to the (pseudo-) periodic solutions of the parametric pendulum in the phase space $\tilde{\eta}_0 < 0$ can propagate.

Using the Floquet-Bloch theorem, the displacement field of a wave in a LUIP medium involving one main periodicity (a SL of the type "ABABABAB" or a medium in which the wave propagation is described by Eq. (4)), is the product of a periodic function times an exponentially (in the BG) or sinusoidally (outside the BG) varying amplitude $A(\tilde{z})$. Assuming some reasonable approximations detailed in Section 2, this amplitude $A(\tilde{z})$ is solution of a wave equation in an hypothetical homogeneous medium with an effective $\tilde{\eta}_0^{eff}$:

$$\frac{d^2A}{d\tilde{z}^2}(\tilde{z}) + \tilde{\eta}_0^{eff} A(\tilde{z}) = 0, \quad (7)$$

$$\tilde{\eta}_0^{eff} = \frac{(\tilde{\eta}_0 - 1)^2 - \tilde{\alpha}\bar{\tilde{\alpha}}}{4}. \quad (8)$$

When equation (7) is derived from equation (4), $\tilde{\eta}_0^{eff}$ is a function of $\tilde{\eta}_0$ and $\tilde{\alpha}$ ($\tilde{\eta}_0^{eff} = \tilde{\kappa}^2$ in Eq. (14) with $\tilde{\beta} = 0$) and its expression is given by equation (8). $\tilde{\eta}_0^{eff}$ is negative for a wave falling in a BG (corresponding to exponential solutions of Eq. (4)), positive otherwise ((pseudo-) periodic solutions) in agreement with the respective exponential and sinusoidal variations of $A(\tilde{z})$.

We hence surmise that $A(\tilde{z})$ will be the solution of a Hill (or Mathieu) equation if $\tilde{\eta}_0^{eff}$ is spatially modulated. In such a case, some propagative solutions $A(\tilde{z})$ are expected in the $\tilde{\eta}_0^{eff} < 0$ region i.e. an inverted pendulum stabilization mechanism for the amplitude $A(\tilde{z})$.

Different designs of periodic medium can provide a modulation of $\tilde{\eta}_0^{eff}$. The simplest way that we have thought about to modulate $\tilde{\eta}_0^{eff}$ and that we will study here is to use a periodic medium composed of two finite periodic subsets: for instance a SSL (see Fig. 1), a SL whose unit cell (length L_e) (e.g. a unit cell of the type "ABABABAB-CDCDCD") contains two finite periodic subsets, the two subsets (periods L_1 and L_2) (e.g. "ABABABAB" and "CDCDCD") having some overlapping regions of their BG. In addition, the relation $L_e \gg L_1, L_2$ is imposed to ensure the separation of scales.

For a wave falling in the overlapping region of the BG, $\tilde{\eta}_0^{eff}$ is negative in each subset but is spatially modulated since different values of $\tilde{\eta}_0^{eff}$ are associated with each subset. By judiciously choosing the size L_e of the SSL, the spatial modulation of $\tilde{\eta}_0^{eff}$ may induce some propagative solutions for the amplitude $A(\tilde{z})$: these solutions would then correspond to the inverted pendulum solutions. The displacement field of the wave, the product of a periodic function times the amplitude $A(\tilde{z})$, would then also be (pseudo-) periodic and thus associated to a propagative wave. In the following, such modes are shown to exist and these unconventional type of waves will be referred as periodic interface modes (PIM).

2 Analytical study in a continuous medium

2.1 Amplitude equation

In this section, assuming some reasonable approximations, an analytical expression of the displacement field of a PIM propagating in a SSL is derived. To this aim, the function $p(z,\omega)$ for a SSL in equation (2), the wave equation in a LUIP medium is first explicit. The Fourier series of the function $p(z,\omega)$ is then restricted to its main relevant harmonics to be able to analytically solve this equation.

Let us consider a SSL whose unit cell is of the type "ABABABABCDCDCD", with the separation of scales $L_e \gg L_1, L_2$. Provided the limitation of the Fourier series of $p(z,\omega)$, a wave equation of the type equation (4) with values of $\tilde{\eta}_0$, $\tilde{\alpha}$ and k_s specific to each subset can be associated to each subset "ABABABAB" or "CDCDCD". At the first order in $\tilde{\alpha}$ [17], the BG of the two subsets can overlap if they are due to a periodic spatial variation of $p(z,\omega)$ at the same wave number $k_s = \frac{2\pi}{L_s}$ with $L_s = \frac{L_1}{m} = \frac{L_2}{n}$ with $m,n \in \mathbb{N}$: the two Fourier transforms of $p(z,\omega)$ associated to each subset should have some peaks at commensurable frequencies. Here, for simplicity, the relation $L_s = L_1 = L_2$ is assumed.

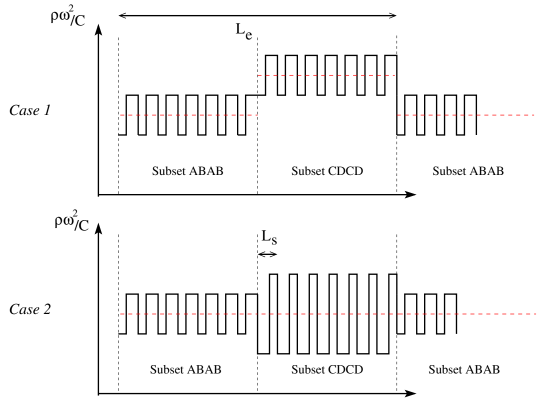

Fig. 3. (Color online) Sketch of the values of $\frac{\rho\omega^2}{C}$ (equal to $p(z,\omega)$ in non singular point) in the SSL in the two limiting cases: *case 1*: the amplitudes of the modulation of $\frac{\rho\omega^2}{C}$ are the same in both subsets while the average values differ; *case 2*: reports the opposite situation. Horizontal red dashed lines report the average values of $\frac{\rho\omega^2}{C}$ in each subset. Vertical dashed lines separate each subset "ABABABAB" and "CDCDCD". For simplicity, the represented case corresponds to $L_s = L_1 = L_2$.

Since in each subset, $\tilde{\eta}_0^{eff}$ (given by Eq. (8)) depends on both $\tilde{\eta}_0$ (proportional to the average value $p(z,\omega)$) and $\tilde{\alpha}$ (proportional to the amplitude of the variation of $p(z,\omega)$), there are two (theoretical) limiting cases that yield a spatial modulation of $\tilde{\eta}_0^{eff}$:

- *case 1:* $\tilde{\eta}_0$ is spatially modulated and $\tilde{\alpha}$ is kept constant
- *case 2:* $\tilde{\eta}_0$ is constant and $\tilde{\alpha}$ is spatially modulated.

Figure 3 reports a sketch of the values of $\frac{\rho\omega^2}{C}$ (equal to $p(z,\omega)$ in a non singular point) in the SSL for both cases. In *case 1*, the amplitudes of the modulation of $\frac{\rho\omega^2}{C}$ are the same in both subsets while the average values differ; *case 2* reports the opposite situation. These two limiting cases can of course be mixed. Nevertheless, for clarity reasons, these cases will be separately treated in the following.

To analytically study the PIM, the Fourier series of the function $p(z,\omega)$ is restricted to its main relevant harmonics.

- *Case 1:* $\tilde{\eta}_0$ is spatially modulated on a length scale L_e and $\tilde{\alpha}$, coefficient of the harmonic at the wave number $k_s = \frac{2\pi}{L_s}$ is kept constant. Since $\tilde{\eta}_0(\omega) = \frac{4p_0(\omega)}{k_s^2}$ in equation (4), a modulation of $\tilde{\eta}_0$ on a length scale L_e

involves an additional harmonic at wave number $k_e = \frac{2\pi}{L_e}$ in the expression of $p(z,\omega)$:

$$p(z,\omega) \approx \left[p_0(\omega) + p_2(\omega)\cos(k_e z)\right] + p_1(\omega)\cos(k_s z), \tag{9}$$

where the quantity $[p_0(\omega) + p_2(\omega)\cos(k_e z)]$ has replaced the term $p_0(\omega)$ in equation (3). Injecting equation (9) in equation (2), $u(\tilde{z})$ is solution of the following modified Mathieu equation:

$$\frac{d^2u}{d\tilde{z}^2} + \left[\tilde{\eta}_0 + \tilde{\alpha}e^{i2\tilde{z}} + \tilde{\beta}e^{i\tilde{k}_e\tilde{z}} + c.c.\right]u = 0, \tag{10}$$

where $\tilde{\eta}_0 = \frac{4p_0(\omega)}{k_s^2} > 0$, $\tilde{\alpha} = \frac{2p_1(\omega)}{k_s^2}$, $\tilde{\beta} = \frac{2p_2(\omega)}{k_s^2}$, $\tilde{k}_e = \frac{2k_e}{k_s}$, $\tilde{z} = \frac{k_s z}{2}$ and where complex quantities have been introduced (*c.c.* means complex conjugates).

– *Case 2:* $\tilde{\eta}_0$ is constant and $\tilde{\alpha}$ coefficient of the harmonic at the wave number $k_s = \frac{2\pi}{L_s}$ is modulated on a length scale L_e. Hence, the main relevant harmonics describing $p(z,\omega)$ are:

$$p(z,\omega) \approx p_0(\omega) + \left[p_1(\omega) + p_2(\omega)\cos(k_e z)\right]\cos(k_s z), \tag{11}$$

where the quantity $[p_1(\omega) + p_2(\omega)\cos(k_e z)]$ has replaced $p_1(\omega)$ in equation (3). Substituting equation (11) in equation (2), the following modified Mathieu equation derives:

$$\frac{d^2u}{d\tilde{z}^2} + \left[\tilde{\eta}_0 + \tilde{\alpha}e^{i2\tilde{z}} + \frac{\tilde{\beta}}{2}e^{i(2-\tilde{k}_e)\tilde{z}} + \frac{\tilde{\beta}}{2}e^{i(2+\tilde{k}_e)\tilde{z}} + c.c.\right]u = 0, \tag{12}$$

where $\tilde{\eta}_0 = \frac{4p_0(\omega)}{k_s^2} > 0$, $\tilde{\alpha} = \frac{2p_1(\omega)}{k_s^2}$, $\tilde{\beta} = \frac{2p_2(\omega)}{k_s^2}$, $\tilde{k}_e = \frac{2k_e}{k_s}$, $\tilde{z} = \frac{k_s z}{2}$ and where complex quantities have been introduced.

The PIM, solutions of equations (10) and (12) are now analysed. Note that a general study of equation (10) can be found in references [22,23]. Here, this study examines if the parametric excitations at wave vector $\tilde{k}_e$ (Eq. (10)) and at wave vectors $2 \pm \tilde{k}_e$ (Eq. (12)) can create some (pseudo-) periodic solutions inside the BG induced by the excitation $e^{\pm i2\tilde{z}}$ (with $\tilde{\beta} = 0$). A wave in the first BG created by the excitation $e^{\pm i2\tilde{z}}$ i.e. $(\tilde{\eta}_0(\omega)-1)^2 < \tilde{\alpha}\bar{\tilde{\alpha}}$ (this condition derives from Eq. (8)) is considered and again, the separation of space scales $\tilde{k}_e \ll 1$ is assumed. The coordinate system of equations (10) and (12) is changed to define the function $A(\tilde{z})$:

$$u(\tilde{z}) = A(\tilde{z})e^{i\tilde{z}} + c.c., \tag{13}$$

where $A(\tilde{z})$, the amplitude of $u(\tilde{z})$ is assumed to slowly vary on the length scale 1 ($\frac{4\pi}{k_s}$ in real units).

– *Case 1:* introducing equation (13) in equation (10), neglecting the second derivative of $A(\tilde{z})$ [24] and using $\tilde{k}_e \ll 1$, the identification of the Fourier components at wave vector 1 and −1, and straightforward calculations yield to the following equation for $A(\tilde{z})$:

$$\frac{d^2A}{d\tilde{z}^2} + \tilde{\kappa}^2A + \left[\frac{\tilde{\eta}_0 - 1}{2}\tilde{\beta}e^{i\tilde{k}_e\tilde{z}} + \frac{\tilde{\beta}^2e^{2i\tilde{k}_e\tilde{z}}}{4} + c.c.\right]A = 0, \tag{14}$$

$$\text{with} \quad \tilde{\kappa}^2 = \frac{(\tilde{\eta}_0 - 1)^2 - \tilde{\alpha}\bar{\tilde{\alpha}} + 2\tilde{\beta}\bar{\tilde{\beta}}}{4}. \tag{15}$$

Equation (14) is a Hill equation i.e. the equation of a parametric oscillator and governs the amplitude $A(\tilde{z})$ of the displacement field.

– *Case 2*: introducing equation (13) in equation (12), $A(\tilde{z})$ is solution of the following equation:

$$\frac{d^2A}{d\tilde{z}^2} + \tilde{\kappa}^2A + \left[\frac{\tilde{\alpha}\bar{\tilde{\beta}} + \bar{\tilde{\alpha}}\tilde{\beta}}{8}e^{i\tilde{k}_e\tilde{z}} + \frac{\tilde{\beta}\bar{\tilde{\beta}}e^{2i\tilde{k}_e\tilde{z}}}{16} + c.c.\right]A = 0, \tag{16}$$

$$\text{with} \quad \tilde{\kappa}^2 = \frac{(\tilde{\eta}_0 - 1)^2 - \tilde{\alpha}\bar{\tilde{\alpha}} - \frac{\tilde{\beta}\bar{\tilde{\beta}}}{2}}{4}. \tag{17}$$

Equation (16) is again a Hill equation. In addition, though the coefficients differ, the harmonics involved in the parametric excitation in equation (16) are the same as the ones in equation (14): solutions of equations (14) and (16) are thus qualitatively equivalent.

Physically, these mathematical similarities evidence that, as suggested previously, the amplitudes $A(\tilde{z})$ have the same qualitative behaviours in both *case 1* and *case 2*, since both cases formally yield to the modulation of η_0^{eff}.

Let us first discuss the solutions of equation (14) (or Eq. (16)) in the specific case $\tilde{\beta} = 0$. As mentioned in the heuristic argument, the amplitude $A(\tilde{z})$ is solution of a wave equation in a hypothetical homogeneous medium with an effective $\tilde{\eta}_0^{eff} = \tilde{\kappa}^2$: equations (7) and (8) are, respectively, equivalent to equations (14) and (16) and to equations (15) and (17) in the case $\tilde{\beta} = 0$. If $\tilde{\kappa}^2 > 0$ (or equivalently $(\tilde{\eta}_0(\omega) - 1)^2 > \tilde{\alpha}\bar{\tilde{\alpha}}$), the solutions $A(\tilde{z})$ are sinusoidal: $u(\tilde{z})$ equation (13) is then a (pseudo-) periodic function involving harmonics at wave vector $1 \pm \tilde{\kappa}$. If $\tilde{\eta}_0^{eff} = \tilde{\kappa}^2 < 0$ (or $(\tilde{\eta}_0(\omega) - 1)^2 < \tilde{\alpha}\bar{\tilde{\alpha}}$), the solutions $A(\tilde{z})$ exponentially vary: the wave falls in the BG created by the excitation $e^{\pm i2\tilde{z}}$. These results corroborate the hypothesis of the second paragraph in Section 1.2.

2.2 Analytical expression of the amplitude $A(\tilde{z})$

In this section, an approximated analytical expression of the amplitude $A(\tilde{z})$ is derived solving equation (14) in the general case $\tilde{\beta} \neq 0$. Solutions of equation (16) can be straightforwardly deduced from this analysis.

In the general case $\tilde{\beta} \neq 0$, equation (14) is similar to a Mathieu equation but involves a periodic excitation composed of a fundamental and one harmonic. Its solutions are similar to the solutions of the Mathieu equation. Noticeably, some periodic solutions exist in the $\tilde{\kappa}^2 < 0$ half-space phase: this result can be shown numerically, if $\frac{2}{\tilde{k}_e}$ is a rational number[1] by calculating the eigenvalues of the propagator of equation (14) (as performed to get Fig. 2b) or analytically provided $|\tilde{\kappa}| \ll \tilde{k}_e$. This latter possibility is detailed below.

Similarly to the resolution of the motion of a particle in a fast oscillating field [25], the solutions of equation (14) write: $A(\tilde{z}) = S(\tilde{z}) + \xi(\tilde{z})$, where ξ is a periodic function varying on the length-scale $\frac{\pi}{\tilde{k}_e}$, while $S(\tilde{z})$ varies on a much longer length scale $\frac{2\pi}{\tilde{k}_\gamma}$ (see below). Introducing this decomposition in equation (14) and identifying the functions varying on each length scale yields:

$$\xi(\tilde{z}) = \left[\frac{\tilde{\eta}_0 - 1}{2\tilde{k}_e^2}\tilde{\beta}e^{i\tilde{k}_e\tilde{z}} + \frac{\tilde{\beta}^2 e^{2i\tilde{k}_e\tilde{z}}}{16\tilde{k}_e^2} + c.c.\right] S(\tilde{z}), \quad (18)$$

$$\frac{d^2S}{d\tilde{z}^2} + \tilde{k}_\gamma^2 S = 0, \quad (19)$$

with $$\tilde{k}_\gamma^2 = \tilde{\kappa}^2 + \frac{(\tilde{\eta}_0 - 1)^2}{2\tilde{k}_e^2}\tilde{\beta}\bar{\tilde{\beta}} + \frac{\tilde{\beta}^2\bar{\tilde{\beta}}^2}{32\tilde{k}_e^2}. \quad (20)$$

Hence, even if $\tilde{\kappa}^2 < 0$, $\tilde{k}_\gamma^2$ can be positive provided $\frac{(\tilde{\eta}_0-1)^2}{2\tilde{k}_e^2}\tilde{\beta}\bar{\tilde{\beta}} + \frac{\tilde{\beta}^2\bar{\tilde{\beta}}^2}{32\tilde{k}_e^2} > |\tilde{\kappa}^2|$: some periodic solutions to equation (14) exist in the $\tilde{\kappa}^2 < 0$ half-space phase: these solutions precisely correspond to the PIM, the transposition of the inverted pendulum case to the propagation of wave in a LUIP medium. These results demonstrate the conjecture made in the third paragraph of Section 1.2. In such case ($\tilde{\kappa}^2 < 0$ and $\tilde{k}_\gamma^2 > 0$), the solution of equation (10) writes:

$$u(\tilde{z}) = A(\tilde{z})e^{i\tilde{z}} + \bar{A}(\tilde{z})e^{i\tilde{z}} + c.c., \quad (21)$$

$$A(\tilde{z}) = A_0 e^{ik_\gamma\tilde{z}}\left[1 + \frac{\tilde{\eta}_0 - 1}{2\tilde{k}_e^2}\tilde{\beta}e^{i\tilde{k}_e\tilde{z}} + \frac{\tilde{\beta}^2 e^{2i\tilde{k}_e\tilde{z}}}{16\tilde{k}_e^2} + c.c.\right], \quad (22)$$

where A_0 is defined from the initial conditions. Equation (21) describes an unconventional type of wave, the PIM. The displacement field $u(\tilde{z})$ of PIM equation (21) is essentially an oscillating function at wave vector 1 (short length scale) in reduced space unit ($\frac{\pi}{L_s}$ in real space unit) whose amplitude $A(\tilde{z})$ is spatially modulated. The function $A(\tilde{z})$ is a periodic function with wave vectors $\tilde{k}_e$ (corresponding to an intermediate length scale) and $2\tilde{k}_e$ whose amplitude $A_0 e^{ik_\gamma\tilde{z}}$ is modulated at the wave vector $\tilde{k}_\gamma$ (corresponding to a large length scale). Note that, from the heuristic arguments (Sect. 1), the amplitude $A(\tilde{z})$ was expected to have some exponential increasing or decreasing (on the intermediate length scale), which is not the case from equation (22). However, the above analytical calculations, based on a perturbation theory at the first order, only provide the main harmonics of the Fourier transform of $u(\tilde{z})$ and elude the non linear terms. As a consequence, the expression of $u(\tilde{z})$ equation (21) as well as the expressions of $\tilde{\kappa}$ equation (15) and of $\tilde{k}_\gamma$ equation (20) are only approximated expressions.

The preceding analytical analysis can be related to the Floquet theory mentioned in Section 1.1. The Floquet theory applies to equation (10) if the parametric excitation $\tilde{\alpha}e^{i2\tilde{z}} + \tilde{\beta}e^{i\tilde{k}_e\tilde{z}} + c.c.$ is a periodic function (let us call $\tilde{L}$ its period) i.e if $\frac{2}{\tilde{k}_e}$ is a rational number: if $\frac{2}{\tilde{k}_e} = \frac{p}{q}$ is an irreducible fraction ($(p,q) \in \mathbb{N}$)) $\tilde{L} = q\frac{2\pi}{\tilde{k}_e} = p\pi$. In such case, equation (21) can be rewritten evidencing a Bloch wave function $\phi_{Bloch}(\tilde{z})$ verifying $\phi_{\text{Bloch}}(\tilde{z} + \tilde{L}) = \phi_{\text{Bloch}}(\tilde{z})$:

$$u(\tilde{z}) = e^{i\tilde{k}_\gamma\tilde{z}}\phi_{\text{Bloch}}(\tilde{z}) + c.c., \quad (23)$$

$$\phi_{\text{Bloch}}(\tilde{z}) = G(\tilde{z})e^{i\tilde{z}} + \bar{G}(\tilde{z})e^{i\tilde{z}} + c.c., \quad (24)$$

$$G(\tilde{z}) = A_0\left[1 + \frac{\tilde{\eta}_0 - 1}{2\tilde{k}_e^2}\tilde{\beta}e^{i\tilde{k}_e\tilde{z}} + \frac{\tilde{\beta}^2 e^{2i\tilde{k}_e\tilde{z}}}{16\tilde{k}_e^2} + c.c.\right].$$

From such an expression, one can show that the eigenvalues of the propagator of equation (10) write $e^{i\tilde{k}_\gamma\tilde{L}}$.

To show the relevance, but also the limit of this analytical derivation, the solution $u(\tilde{z})$ of equation (10) for $\tilde{\alpha} = \bar{\tilde{\alpha}} = 0.1$, $\tilde{\beta} = \bar{\tilde{\beta}} = 0.05$, $\tilde{k}_e = \frac{1}{14}$ and $\tilde{\eta}_0 = 1.066$ are examined as an example. On one hand, within these values, $(\tilde{\eta}_0 - 1)^2 < \tilde{\alpha}\bar{\tilde{\alpha}}$, $\tilde{\kappa}^2 < 0$ and $k_\gamma^2 > 0$: the analytical calculation predicts that this wave is in the BG created by the harmonic at $e^{\pm i2\tilde{z}}$, but is periodic due to the presence of the parametric excitation at wave vector $\tilde{k}_e$. On the other hand, equation (10) is numerically solved using standard numerical libraries[2] and the result $u(\tilde{z})$ is reported in Figure 4. Figure 4 represents a function that can be described by equation (21). The function $u(\tilde{z})$ shows three characteristic lengths $\tilde{\lambda}_s$, $\tilde{\lambda}_e$ and $\tilde{\lambda}_\gamma$ defined on Figure 4. $\tilde{\lambda}_s$, the short length scale between two consecutive local maxima of $u(\tilde{z})$ is about 2π in agreement with the analytical prediction. The distance $\tilde{\lambda}_e$ between two local maxima of the amplitude of $u(\tilde{z})$, the intermediate length scale is equal to $14\tilde{\lambda}_s$ so that, $\frac{2\pi}{\tilde{\lambda}_e} = \frac{1}{14} = \tilde{k}_e$ in agreement with the analytical calculations. Finally, the values of the local maxima of the amplitude of $u(\tilde{z})$ are modulated on a large length scale $\tilde{\lambda}_\gamma$, this length scale is expected to be $\frac{2\pi}{\tilde{k}_\gamma}$ from the analytical calculations. If the values of $\tilde{\lambda}_s$ and $\tilde{\lambda}_e$ on Figure 4 are in good agreement with the analytical calculations, the theoretical value derived from equation (20) $\tilde{\lambda}_\gamma^{theo} = 204.4$ significantly under-estimates the value of $\tilde{\lambda}_\gamma \approx 710$ measured from Figure 4 (this latter one can accurately be calculated from the eigenvalues of the propagator of Eq. (10)): the non-linear terms and the different

[1] The Floquet theory applies to equation (10) if the parametric excitation $\tilde{\alpha}e^{i2\tilde{z}} + \tilde{\beta}e^{i\tilde{k}_e\tilde{z}} + c.c.$ is a periodic function i.e. the ratio $\frac{2}{\tilde{k}_e}$ of the excitation wave vectors is a rational number.

[2] A method based on the 4th order Merson's method and the 1st order multi-stage method of up to and including 9 stages with stability control is used.

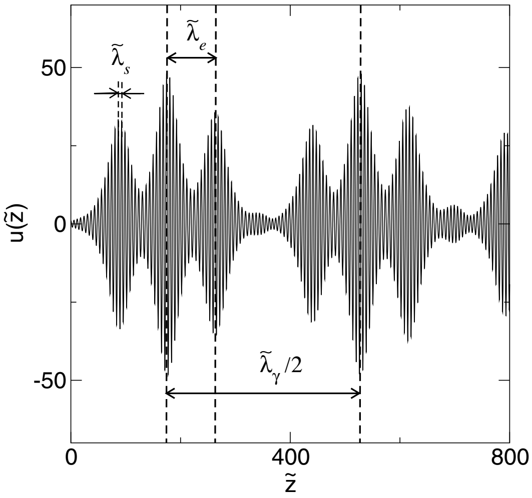

Fig. 4. Function $u(\tilde{z})$ solution of equation (10) for $\tilde{\alpha} = 0.1$, $\tilde{\beta} = 0.05$, $\tilde{k}_e = \frac{1}{14}$ and $\tilde{\eta}_0 = 1.066$ with initial conditions $u(0) = 1$ and $\frac{du}{d\tilde{z}}(0) = 0$. The vertical dashed lines reveal the characteristic lengths of the variation of $u(\tilde{z})$: $\tilde{\lambda}_s$, $\tilde{\lambda}_e$ and $\tilde{\lambda}_\gamma$.

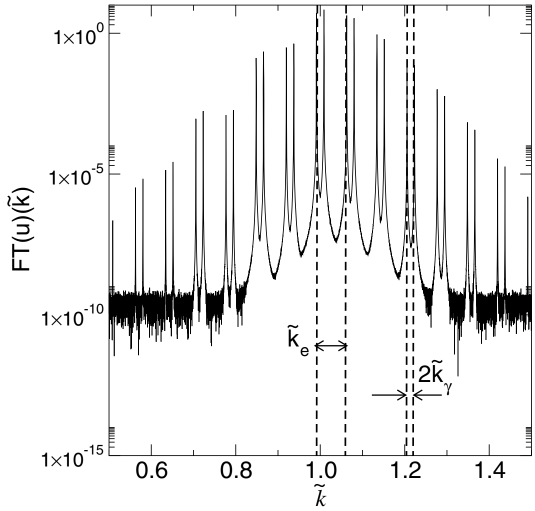

Fig. 5. Fourier transform (semi-log plot) $\mathrm{FT}(u)(\tilde{k})$ of the solution of equation (10) for $\tilde{\alpha} = 0.1$, $\tilde{\beta} = 0.05$, $\tilde{k}_e = \frac{1}{14}$ and $\tilde{\eta}_0 = 1.066$ with initial conditions $u(0) = 1$ and $\frac{du}{d\tilde{z}}(0) = 0$. The vertical dashed lines reveal some of the characteristic wave vectors involved in the variation of $u(\tilde{z})$: $\tilde{k}_e$ and $\tilde{k}_\gamma$.

harmonics can not be neglected in order to obtain a quantitative result.

This analysis can be enriched by a Fourier analysis of $u(\tilde{z})$. Figure 5 reports the Fourier transform $\mathrm{FT}(u)(\tilde{k})$ of the function $u(\tilde{z})$ for $\tilde{k} \in [0.5, 1.5]$. The spectrum of $u(\tilde{z})$ shows some wide features composed of many peaks around $\tilde{k} = 2n + 1$ with $n \in \mathbb{N}$. Since the analytical expression (21) has neglected the non-linear terms and thus only provides the harmonics around $\tilde{k} \approx 1$, Figure 5 only shows the features around $\tilde{k} = 1$. The discussion below focus on the harmonics around $\tilde{k} \approx 1$. The values of $\tilde{k}_e$ and $\tilde{k}_\gamma$ can be recovered from the differences of spatial frequencies between the peaks around $\tilde{k} \approx 1$. As suggested by equation (21), the spectrum of $u(\tilde{z})$ is expected to show some peaks at frequencies $1 \pm \tilde{k}_\gamma$, $1 \pm \tilde{k}_e \pm \tilde{k}_\gamma$ and $1 \pm 2\tilde{k}_e \pm \tilde{k}_\gamma$: an example of the peaks to be considered in order to measure the values $\tilde{k}_e$ and $\tilde{k}_\gamma$ is reported in Figure 5. Naturally, the values of $\tilde{k}_e$ and $\tilde{k}_\gamma$ measured from Figure 5 agree with the values $\tilde{\lambda}_e$ and $\tilde{\lambda}_\gamma$ measured in Figure 4 in the real space. Note that, due to the non-linear terms and the different harmonics eluded in the analytical calculations, Figure 5 shows some additional frequencies at $1 \pm m\tilde{k}_e \pm \tilde{k}_\gamma$ with $m \in \mathbb{N}$.

Though a very rough estimate of $\tilde{k}_\gamma$ (or $\tilde{\lambda}_\gamma$) and some missing harmonics, the analytical derivation and equation (21) provide a relevant description of the PIM, the unconventional type of waves that transposes the case of the inverted pendulum to the wave.

3 Layered systems

Though theoretically relevant to study the PIM, equations (10) or (12) are hardly applicable for a realistic periodic system: it is actually technically difficult to create a material with a controlled gradient of the sound speed. For these reasons, the systems based on layered structures initially mentioned in Section 1, more easily achievable in experiments will be examined in this section. The propagation of elastic waves in a SSL is considered. To engineer a SSL displaying some PIM, the two limiting cases sketched in Figure 3 can been considered. The *case 1* inevitably requires the use of 3 or 4 different materials. While it seems that the same rule applies for *case 2*, it is, however, possible to benefit from the presence of the several BG in each subset to engineer a SSL displaying some PIM using only two different materials. This latter case is examined in the following. Technically, due to the generally different lattice mismatch of materials, it is more challenging (though not impossible) to create a (quasi-) perfect SSL based on three or four materials than a one based on two materials.

3.1 Dispersion diagram and periodic interface modes

The propagation of elastic waves in a SSL (period L_e) (see Fig. 1) whose elementary unit cell is composed of $10 + x$ periods of a SL referred as SL1 with $x = 0.5$ and 10 periods of another SL referred as SL2 is studied. The unit cell of SL1 (period L_1) is composed of 5.65 nm (10 monolayers (ML)) of GaAs and 2.26 nm (4ML) of AlAs SL, while the one of SL2 (period L_2) is composed of 11.3 nm (20ML) of GaAs and 4.52 nm (8ML) of AlAs. The (001) crystalline directions of the GaAs and AlAs crystal are perpendicular to the layers for both SL1 and SL2. The period of SL1 is thus $L_1 = 7.91$ nm, while the one of SL2 is $L_2 = 15.82$ nm. Finally the period of the SSL is $L_e = 241.26$ nm. The SL1 and SL2 parameters have been chosen so that both SL1 and SL2 have an overlapping BG. The period L_e of the SSL has been chosen so that

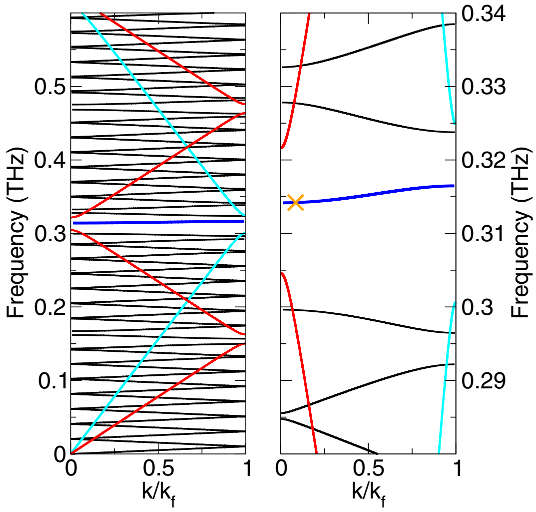

Fig. 6. (Color online) Dispersion diagram of the SSL (black), SL1 (cyan) and SL2 (red) between 0–0.6 THz (a) and 0.28–0.34 THz (b), the x-axis reports the Bloch wave vector normalized by $k_f = \frac{\pi}{\Xi}$ with $\Xi = L_e$(SSL), L_1(SL1) or L_2(SL2). The y-axis reports the frequency $\nu = \frac{\omega}{2\pi}$. The blue curve and orange cross point up a PIM band and the PIM mode at $\nu = 0.3142$ THz (see Fig. 7).

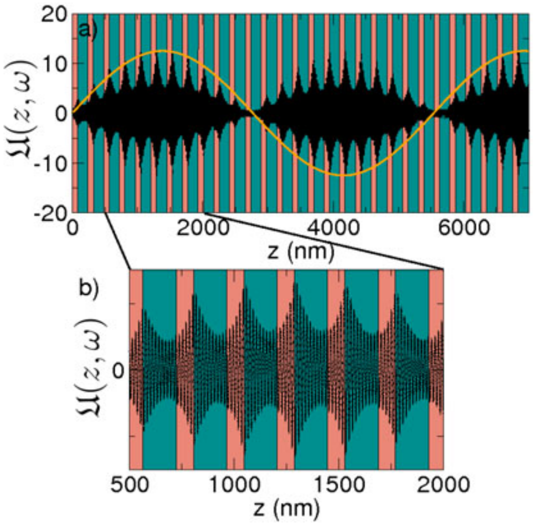

Fig. 7. (Color online) Displacement fields $\mathfrak{U}(z,\omega)$ solutions of equation (1) in the SSL for $\nu = \frac{\omega}{2\pi} = 0.3142$ THz between 0–7000 nm (a) and 500–2000 nm (b). The dark green and red background colors identify the SL1 and SL2 regions. An orange curve, a guide to the eye emphasizes the oscillations at the Bloch wave vector.

some PIM appear in the overlapping region of the SL1 and SL2 BG. The overlapping region that will be considered in the following, corresponds to the first BG of SL1 and to the second one of SL2. In SL1, the first BG is essentially created by the first harmonic of $p(z,\omega)$ at $k_s = \frac{2\pi}{L_1}$ (i.e. $\lambda_s = L_1$), while in SL2, the second BG is essentially created by the second harmonic of $p(z,\omega)$ at $k_s = 2\frac{2\pi}{L_2} = \frac{2\pi}{L_1}$ [17]. This configuration corresponds to the *case 2* mentioned in Section 2 i.e. a spatial modulation of the coefficient of the harmonic at k_s and the same average value of $p(z,\omega)$ in each subset.

Considering wave vectors with normal incidence, Figure 6 reports the dispersion diagrams of the SSL, SL1 and SL2 and, Figure 6b a zoom in the frequency range 0.28 THz–0.34 THz, corresponding to an overlapping region of the SL1 and SL2 BG. These dispersion diagrams are calculated from the transfer matrix method [26], a representation of the propagator of equation (1) in these systems. The following numeric values have been used for the calculation: $\rho_{GaAS} = 5317.6$ Kg m^{-3}, $\rho_{AlAS} = 3760$ Kg m^{-3}, $C_{GaAS} = 118.8$ GPa and $C_{AlAS} = 119.2$ GPa.

In Figures 6a and 6b, the multiple foldings and the mini-BG created by the periodicity L_e of the SSL appear. More interestingly, the SSL phase diagram shows some phonons (blue curve in Fig. 6) in the overlapping region of the SL1 and SL2 BG. As shown below, these phonons are PIM. Figure 7 reports the displacement field $\mathfrak{U}(z,\omega)$, solution of equation (1) in the SSL for $\nu = \frac{\omega}{2\pi} = 0.3142$ THz, a PIM identified by an orange cross in Figure 6b. Though in the BG of both SL1 and SL2, this solution describes a (pseudo-) periodic mode that propagates in the LUIP medium. $\mathfrak{U}(z,\omega)$ is an oscillating function and the distance between two consecutive local maxima is about 15.95 nm (short length scale), in good agreement with the value of $2L_s = 2L_1 = L_2$. This distance has been deduced from the distance between three consecutive maxima around $z = 840$. Since $\mathfrak{U}(z,\omega)$ involves many harmonics as it will be shown below, the apparent period of these oscillations on the short length scale can slightly vary depending on the position where they are measured. The amplitude of these oscillations are alternatively exponentially increasing and decreasing in SL1 and SL2: the distance between two consecutive local maxima of the amplitude is the period of the SSL, $L_e = 241.26$ nm, the intermediate length scale. Finally, the maxima of this amplitude are modulated by a sinusoidal envelope on a large length scale. From the distance between three consecutive maxima of this envelope, the period of this oscillation is deduced to be 5730 nm. An orange curve, a guide to the eye emphasizes these oscillations on Figure 7.

Due to the weak difference between the AlAs and GaAs stiffnesses [27], $u(z,\omega) \approx \mathfrak{U}(z,\omega)$, and $p(z,\omega) \approx \frac{\omega^2\rho(z)}{C}$ in equation (2). The displacement field $\mathfrak{U}(z,\omega)$ is similar to the displacement field shown in Figure 4 of Section 2 though the ratios between the different length scales (short/intermediate and intermediate/large length scales) differ.

The displacement field $\mathfrak{U}(z,\omega)$ can be described by equation (21). The oscillation on the short length scale with a period of about 15.95 nm corresponds to the $e^{i\pm\tilde{z}}$ (in reduced unit or $e^{\pm i\frac{\pi z}{\lambda_s}}$ in real space unit) terms in equation (21): the period actually corresponds to $2\lambda_s = 2L_1 = L_2 = 15.82$ nm. The intermediate length scale is related to the exponential variation of the wave amplitude and corresponds to the $e^{\pm i\tilde{k}_e\tilde{z}}$ (in reduced unit or $e^{\pm ik_e z}$ in real space unit) terms in equation (21).

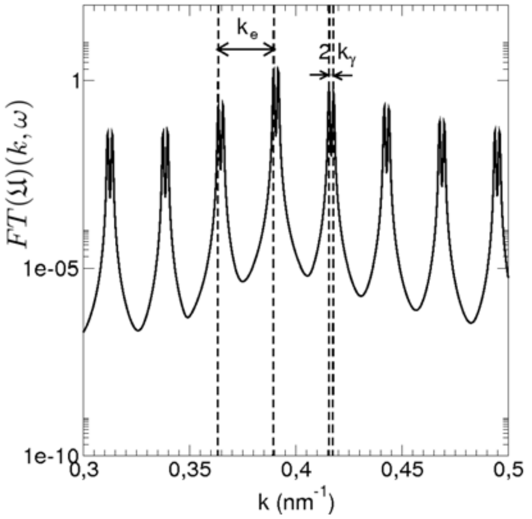

Fig. 8. Fourier transform (semi-log plot) of the displacement field $\mathrm{FT}(\mathfrak{U})(k,\omega)$ in the SSL for $\nu = \frac{\omega}{2\pi} = 0.3142$ THz as a function of the wave vector. The vertical dashed lines reveal some of the characteristic wave vectors involved in the variation of $\mathfrak{U}(z,\omega)$: $\tilde{k}_e$ and $\tilde{k}_\gamma$.

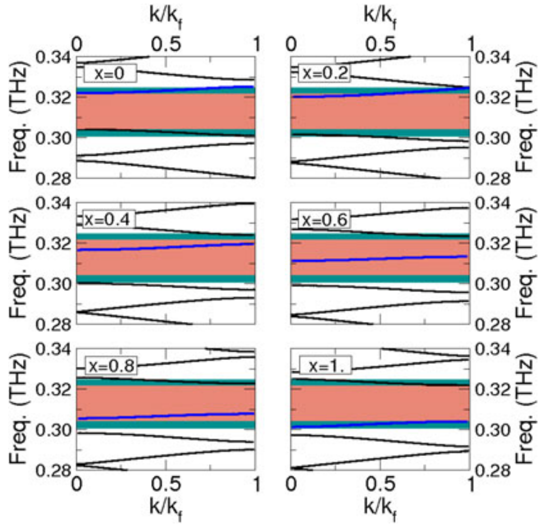

Fig. 9. (Color online) Dispersion diagram of the SSL (black and blue curves) between 0.28–0.34 THz as a function of x. The BG of SL1 and SL2 are represented by the cyan+red and red regions.

Finally, the variation on the large length scale, 5730 nm from Figure 7 corresponds to the $e^{\pm i\tilde{k}_\gamma \tilde{z}}$ (in reduced unit or $e^{\pm i k_\gamma z}$ in real space unit with $\tilde{k}_\gamma = \frac{2k_\gamma}{k_s}$) terms in equation (21). The value of this large length scale can also be obtained from the Bloch wave vector $k_\gamma = 0.0846 k_f = 0.001102$ nm^{-1} ($\frac{2\pi}{k_\gamma} = 5703$ nm) of the SSL mode at $\nu = \frac{\omega}{2\pi} = 0.3012$ THz (orange cross) in the dispersion diagram Figure 6b: this value derives from the eigenvalues of the transfer matrix. The weak difference (of the order of 0.4%) between the values obtained from the direct measure of the period or from the Bloch wave vector are related to numerical precisions.

The displacement field reported in Figure 7 can also be considered in the Fourier space. Figure 8 reports the Fourier transform $\mathrm{FT}(\mathfrak{U})(k,\omega)$ of the displacement fields $\mathfrak{U}(z,\omega)$ as a function of the wave number k between 0.3 and 0.5 nm^{-1}. The spectrum of the displacement fields $\mathfrak{U}(z,\omega)$ is analogous to the one reported in Figure 5 and shows some wide features composed of numerous peaks around the wave numbers $k = 0.392(2n+1)$ nm^{-1} with $n \in \mathbb{N}$: similarly to the analyse performed in Section 2, the feature around $k = 0.392$ nm^{-1} is examined and the full spectrum is not represented in Figure 8.

The oscillation on the short length scale exhibited in Figure 7b corresponds to the wide feature around the wave number 0.392 nm^{-1} (wave number of the highest peak), corresponding to a period 16.02 nm. Analysing Figure 8 with the help of equation (21) and Figure 5, the intermediate and large length scales can be deduced from the distances between the peaks of Figure 8. (i) On the intermediate length scale, the distance between the two peaks mentioned on Figure 8, $k_e = \frac{2\pi}{L_e} = 0.026$ nm^{-1} i.e. a period of 241.66 nm, corresponds to the period L_e of the SSL. (ii) The large length scale deduces from the distance between two others peaks mentioned on Figure 8: $\tilde{k}_\gamma \approx 0.0011$ nm^{-1}, e.g. a period of 5710 nm in good agreement with the results found in the real space. The difference between the measures in real and Fourier space should be regarded considering the uncertainty $\Delta k = 1.5e-4$ nm^{-1} in the Fourier space due the finite integration range used in the calculation of the Fourier transform.

The wave reported in Figure 7 and its Fourier transform Figure 8 are similar to the PIM evidenced in Section 2 represented in Figure 4 and its Fourier transform Figure 5. These similarities show the relevance of the analytic analysis of Section 2. As a conclusion to this section, the unconventional type of waves, the PIM has been evidenced in experimentally achievable structures. These PIM transpose the case of the inverted pendulum to the case of elastic waves (with zero in-plane wave vector) in a layered structure. These unconventional waves can relevantly be described by analytical expression (21).

3.2 Control of the PIM frequencies

Beyond the existence of the PIM, it is possible to fully control their frequencies from the engineering of the SSL by using a fractional number of the periods of SL1 or SL2 [7]. Some SSL formed by $10+x$ periods of SL1 and 10 periods of SL2 with different x values between 0 to 1 are considered. Figure 9 reports the dispersion diagrams of these SSL between 0.28–0.34 THz for $x = 0$, 0.2, 0.4, 0.6, 0.8 and 1. In each of these diagrams, the BG of SL1 and SL2 are represented using cyan + red and red regions. In addition, a SSL frequency band is pointed out by distinguishing it from the others by a blue curve in the dispersion diagram. Figure 9 shows that this frequency band continuously shifts from above to below the overlapping region of the SL1 and SL2 BG while increasing x. Hence, for each value of x, all or part of the modes in this band are in the overlapping regions of the SL1 and SL2 BG, and hence correspond to some PIM. The frequencies of the PIM can thus be tuned by judiciously choosing the unit cell structure and more precisely the value of x.

4 Discussion

As shown, the PIM are the transposition of the inverted pendulum case to the propagation of elastic waves (with a zero in-plane wave vector). The concept of this transposition, to use a periodic structure involving two main (judiciously chosen) periods is general and can be applied to any kind of waves (elastic, electromagnetic, etc.) as soon as they are solutions of a wave equation: indeed, the derivation done in Section 2 is not specialized to the case of phonons. As already mentioned, some unconventional waves analogous to PIM have already been evidenced in different fields of the physics, though not interpreted as the transposition of the inverted pendulum case: all the examples below have already been cited in the introduction. The existence of interface optical phonons [9] in SLs are related to PIM: the atomic potential, that mimics the term $e^{2i\tilde{z}}$ in equation (10) induces the BG between the acoustic and optical phonons branches; the SL periodicity corresponding to the term $e^{i\tilde{k}_e\tilde{z}}$ in equation (10), creates the parametric excitation that stabilizes some phonons in this BG. The description of interface optical phonons involves the coupling between EM waves and polar phonons through a frequency-dependent dielectric constant that accounts for the atomic potential: the theoretical description of these modes is thus essentially similar to the description of the amplitude $A(\tilde{z})$ in equation (14) where the term $\tilde{\kappa}^2$ would be proportional to a frequency-dependent dielectric constant [10].

The propagation of wave in a CROW [11,12] can be described in the framework reported in this manuscript: indeed, the periodicity of the photonic crystal induces a BG that can be related to the term $e^{2i\tilde{z}}$ in equation (10), and the periodic presence of impurities (cavities) to the term $e^{i\tilde{k}_e\tilde{z}}$. This latter excitation, if judiciously chosen (partly by choosing the size of the cavity) results in the appearance of some propagative waves in the BG of the photonic crystal.

Finally, as already mentioned, optical Tamm states are equivalent to PIM. The SSL and the PIM, described in the present work are equivalent to the photonic crystal and optical Tamm state described in references [14–16].

5 Conclusion

As a conclusion, the propagation of waves in LUIP media is closely related to the physics of the parametric oscillator. The transposition of the inverse parametric pendulum to the case of waves (with a zero in-plane wave vector) exhibits an unconventional type of waves: the case of phonons has been considered here evidencing the PIM. A different approach [14–16] applied to the case of electromagnetic waves, has evidenced the optical Tamm states. The PIM and optical Tamm states are qualitatively equivalent. PIM have been theoretically described using a formalism derived from the parametric oscillator. Finally, a realizable structure evidencing these PIM has been given.

Due to the highly localized nature of the displacement field of PIM, the SSL are expected to be useful in the investigation of non-linear effects or in the realization of materials involving a high electron-phonon coupling [28].

Finally, the transposition of the inverse parametric pendulum has been considered here in the case of elastic waves in an unidimensional structure to exhibit the PIM. Due to its generality, the transposition of the inverse parametric pendulum to any kind of waves (spin, capillary waves . . .) can be considered. In addition, though we have focussed on an unidimensional system, the generalization of the described concept to two- and three-dimensional devices is worth being considered.

The author thanks J. Morillo, M. Benoit, A. Ponchet and J.R. Huntzinger for useful discussions.

References

1. E. El Boudouti, B. Djafari-Rouhani, A. Akjouj, L. Dobrzynski, Surf. Sci. Rep. **64**, 471 (2009)
2. E. Istrate, E.H. Sargent, Rev. Mod. Phys. **78**, 455 (2006)
3. N. Ashcroft, N.D. Mermin, *Solid State Physics* (Holt, Rinehart and Winston, 1976)
4. M. Steslicka, R. Kucharczyk, A. Akjouj, B. Djafari-Rouhani, L.D.S.G. Davison, Surf. Sci. Rep. **47**, 92 (2002)
5. B. Djafari-Rouhani, L. Dobrzynski, O.H. Duparc, R.E. Camley, A.A. Maradudin, Phys. Rev. B **28**, 1711 (1983)
6. R.E. Camley, B. Djafari-Rouhani, L. Dobrzynski, A.A. Maradudin, Phys. Rev. B **27**, 7318 (1983)
7. E.H. El Boudouti, B. Djafari-Rouhani, E.M. Khourdifi, L. Dobrzynski, Phys. Rev. B **48**, 10987 (1993)
8. D. Bria, E.H. El Boudouti, A. Nougaoui, B. Djafari-Rouhani, V.R. Velasco, Phys. Rev. B **60**, 2505 (1999)
9. A.K. Sood, J. Menéndez, M. Cardona, K. Ploog, Phys. Rev. Lett. **54**, 2115 (1985)
10. R.E. Camley, D.L. Mills, Phys. Rev. B **29**, 1695 (1984)
11. A. Yariv, Y. Xu, R.K. Lee, A. Scherer, Opt. Lett. **24**, 711 (1999)
12. Y.H. Ye, J. Ding, D.Y. Jeong, I.C. Khoo, Q.M. Zhang, Phys. Rev. E **69**, 056604 (2004)
13. F. Villa, J. Gaspar-Armenta, Opt. Express **12**, 2338 (2004)
14. A.V. Kavokin, I.A. Shelykh, G. Malpuech, Phys. Rev. B **72**, 233102 (2005)
15. T. Goto, A.V. Dorofeenko, A.M. Merzlikin, A.V. Baryshev, A.P. Vinogradov, M. Inoue, A.A. Lisyansky, A.B. Granovsky, Phys. Rev. Lett. **101**, 113902 (2008)
16. T. Goto, A.V. Baryshev, M. Inoue, A.V. Dorofeenko, A.M. Merzlikin, A.P. Vinogradov, A.A. Lisyansky, A.B. Granovsky, Phys. Rev. B **79**, 125103 (2009)

17. N. Combe, J.R. Huntzinger, J. Morillo, Eur. Phys. J. B **68**, 47 (2009)
18. D. Bria, B. Djafari-Rouhani, Phys. Rev. E **66**, 056609 (2002)
19. L. Landau, E. Lifchitz, *Elasticity Theory*, 2nd edn. (Mir, Moscow, 1967)
20. C. Viterbo, in *Cours Ecole Polytechnique* (2007)
21. P. Kapitza, in *Collected Papers by P.L. Kapitza*, edited by D.T. Haar (Pergamon Press, 1965), Vol. 2, p. 714
22. S.H. Davis, S. Rosenblat, SIAM J. Appl. Math. **38**, 139 (1980)
23. R.S. Zounes, R.H. Rand, SIAM J. Appl. Math. **58**, 1094 (1998)
24. P. Castiglione, M. Falcioni, A. Lesne, A. Vulpiani, *Chaos and Coarse Graining in Statistical Mechanics* (Cambridge University Press, Cambridge, 2008)
25. L. Landau, E. Lifchitz, *Mechanics*, 3rd edn. (Mir, Moscow, 1969)
26. J. He, B. Djafari-Rouhani, J. Sapriel, Phys. Rev. B **37**, 4086 (1988)
27. M. Trigo, T.A. Eckhause, M. Reason, R.S. Goldman, R. Merlin, Phys. Rev. Lett. **97**, 124301 (2006)
28. I.E. Psarobas, N. Papanikolaou, N. Stefanou, B. Djafari-Rouhani, B. Bonello, V. Laude, Phys. Rev. B **82**, 174303 (2010)